

MGCNN: a learnable multigrid solver for linear PDEs on structured grids

Yan Xie, Minrui Lv, Chensong Zhang
 the State Key Laboratory of Scientific and Engineering Computing
 Beijing
 {xieyan2021, lvminrui, zhangcs}@lsec.cc.ac.cn

Tuesday 19th December, 2023

Abstract

This paper presents a learnable solver tailored to solve discretized linear partial differential equations (PDEs). This solver requires only problem-specific training data, without using specialized expertise. Its development is anchored by three core principles: (1) a multilevel hierarchy to promote rapid convergence, (2) adherence to linearity concerning the right-hand side of equations, and (3) weights sharing across different levels to facilitate adaptability to various problem sizes. Built on these foundational principles, we introduce a network adept at solving PDEs discretized on structured grids, even when faced with heterogeneous coefficients. The cornerstone of our proposed solver is the convolutional neural network (CNN), chosen for its capacity to learn from structured data and its similar computation pattern as multigrid components. To evaluate its effectiveness, the solver was trained to solve convection-diffusion equations featuring heterogeneous diffusion coefficients. The solver exhibited swift convergence to high accuracy over a range of grid sizes, extending from 31×31 to 4095×4095 . Remarkably, our method outperformed the classical Geometric Multigrid (GMG) solver, demonstrating a speedup of approximately 3 to 8 times. Furthermore, we explored the solver’s generalizability to untrained coefficient distributions. The findings showed consistent reliability across various other coefficient distributions, revealing that when trained on a mixed coefficient distribution, the solver is nearly as effective in generalizing to all types of coefficient distributions.

Keywords learnable multigrid solver · convolutional neural network (CNN) · heterogeneous coefficient · convection-diffusion equations

1 Introduction

1.1 Background

Iterative methods play a pivotal role in solving linear systems arising from the discretization of partial differential equations (PDEs). Renowned for their low complexity, parallel scalability, and the flexibility to fine-tune accuracy during iterations, these methods are commonly preferred for large-scale problems. However, no universally efficient iterative method exists for all types of linear systems; their efficacy is intrinsically linked to the specific problem. The creation of an effective iterative method usually involves expert knowledge and significant trial-and-error. The emergence of deep learning has revolutionized multiple sectors, notably computer vision [1, 2, 3], natural language processing [2, 4, 5, 6], and bioinformatics [7, 8, 9]. This trend towards data-driven methodologies is reshaping problem-solving strategies, a shift that is increasingly influencing numerical methods for solving PDE problems, as evidenced by recent developments in the field.

Broadly speaking, deep learning is applied in two ways to solve PDEs. The first approach involves integrating neural networks into traditional algorithms, replacing certain modules. These modules are often tailored to specific problems or based on empirical knowledge. The goal is to enhance the performance of classical algorithms. For instance, neural networks have been used to pinpoint discontinuity locations [10],

introduce artificial viscosity for stabilization [11], refine multigrid methods [12, 13], and identify optimal initial values for nonlinear problems [14].

The second approach to applying deep learning in PDE solving involves using neural networks in roles akin to traditional PDE solvers. A prominent stream within this category is the Physics-Informed Neural Networks (PINNs) [15]. PINNs essentially employ neural networks to approximate the solution of a PDE. This is achieved through minimizing a residual loss that is informed by physical laws, thus adhering to the constraints of various physical equations and boundary conditions. The strength of PINNs lies in their ability to tackle high-dimensional problems and manage complex geometries, owing to their mesh-free nature. This approach has been successfully applied in a range of scenarios, such as solving both forward and inverse problems [16, 17, 18, 19, 20, 21, 15]. Their solve phase lies in training parameters for the network to approximate the solution function.

In our study, we align with the second approach of employing deep learning for PDEs, focusing on a data-driven algorithm that meets problem-specific needs. And we dive into another stream to develop a network capable of learning an operator to solve the problem during inference. While there has been research on operator learning for continuous PDEs [22, 23, 24], our interest lies in creating a solver for discretized linear systems. There already exist solvers capable of solving the given problem in a single [25, 26, 27, 28] or multiple iterative [29, 30, 31, 32, 33, 34] applications of a feed-forward network.

1.2 Related Works

Classical numerical solvers for PDEs typically utilize a multilevel structure to ensure quick convergence and scalability, especially for larger problem sizes. Inspired by this, we aim to replicate a similar multilevel structure in our solver network. Within the current learning framework, the convolutional neural network (CNN) [35] stands out as the most feasible network architecture for this purpose. Consequently, we have chosen the CNN as the main building block of our proposed solver. This decision also guides our focus to problems that are discretized on structured grids, aligning with the inherent capabilities of CNNs.

This concept of integrating a multilevel structure into neural networks has parallels in the field of image processing, particularly in architectures like U-net [36], which have effectively implemented similar strategies. In fact, the work by He et al. [37] elucidated the connection between convolutional neural networks (CNNs) and multigrid algorithms, paving the way for the creation of MgNet. In the realm of numerical PDE solvers, there have been notable efforts to develop CNN-based multigrid neural networks. For example, Chen et al. [32] introduced Meta-MgNet, a model capable of adapting to varying problem parameters. Azulay et al. [33] and Lerer et al. [34] integrated neural networks with the classical shift Laplacian method; they trained these networks on multi-level smooth right-hand-side datasets, enabling them to act as preconditioners for the Flexible Generalized Minimal Residual (FGMRES) method. This approach was particularly effective in solving the Helmholtz equation on heterogeneous media.

Moreover, the success of Google’s GraphCast [38] has further influenced our research, encouraging us to explore Artificial Intelligence (AI) as a potential multigrid solver in this field.

1.3 Our Contributions

In our endeavor to create a learnable solver for discretized linear PDEs, we anchor our design on three key principles: (1) employing a multi-level hierarchical computation structure, (2) implementing the network linearly on the right-hand side of equations, and (3) sharing weights across different levels of the structure. For problems set on structured grids, we observe that Meta-MgNet [32] aligns with the first two principles. However, it’s not tailored for heterogeneous problems.

Other studies, such as those by Azulay et al. [33] and Lerer et al. [34], have developed neural networks for heterogeneous Helmholtz problems. These adhere primarily to the first principle and necessitate integrating the shift Laplacian method during both training and solving phases. Significantly, to the best of our knowledge, there appears to be a gap in existing research concerning the third principle. This principle, the sharing of weights across levels, is crucial for our goal of scaling the network to tackle larger problem sizes efficiently.

Adhering to our established principles and tailored to our specific problem context, we have developed a unique network trained to address the convection-diffusion equation with heterogeneous coefficients. When implemented within the stationary iteration method, our variously hyperparameter-tuned solvers consistently

demonstrate rapid convergence and high accuracy across a range of grid sizes, up to 4095×4095 . Our method achieves a speedup of approximately 3 to 8 times compared to a Geometric Multigrid (GMG) solver on a GPU. This accomplishment underscores the potential of neural networks in effectively resolving large, sparse linear systems derived from discretized PDEs, without the need for additional expert input. It marks a significant stride in the utilization of neural networks for solving complex mathematical problems, particularly in the realm of PDEs.

The rest of this paper is organized as follows: Section 2 lays out the necessary preliminaries and fundamental concepts that form the basis of our study. The terminologies established in this section are consistently employed throughout the paper. Section 3 offers an in-depth discussion of our proposed methodology. In Section 4, we conduct a series of experiments to demonstrate the effectiveness and reliability of our approach. The paper concludes with Section 5, where we summarize our findings and contemplate future avenues of research. For additional insights and detailed information, readers are directed to the appendix.

2 Preliminaries and Notations

In this section, we lay the groundwork for our study by introducing the core concepts and methodologies. We start with the multigrid algorithm, a multi-level iterative method for solving linear systems derived from certain PDE systems. Next, we explore the intricacies of convolutional neural networks and their variant, transposed convolutional neural networks. These discussions are crucial for appreciating the neural network architecture we utilize. Additionally, we present the extension of the Residual Network (ResNet) to a multigrid framework, an essential aspect of our methodology. We conclude this section with the discretization method for the convection-diffusion equation, which serves as our test problem. These preliminary concepts are essential for understanding the methodology, experiments, and results presented in the subsequent sections.

2.1 Iterative Methods

In the context of a linear system $Ax = rhs$, where A is a square matrix, x is the solution vector, and rhs is the right-hand-side vector, the objective of a linear solver is to find the solution x that meets satisfactory tolerance. We can obtain it by directly solving the equation or iteratively enhancing the solution’s accuracy. The latter approach is often preferred due to its lower complexity and potential for parallelization.

One such iterative method is the stationary iteration method, which solves linear systems by iteratively addressing the residual equation $Ax = r$, where $r = rhs - Ax$ represents the residual vector. This method can be defined as follows:

$$x^{k+1} = x^k + Br^k = x^k + B(rhs - Ax^k), \tag{1}$$

where x^k is the solution at the k -th iteration and B serves as the solver, providing an approximate error correction for each residual r^k . To avoid confusion with the term ResNet, we also refer to r^k as the right-hand-side term.

The Krylov subspace method [39] represents another iterative framework where B serves as a preconditioner. This method often accelerates the iteration process despite introducing some overheads. Notable examples include

- the Conjugate Gradient (CG) method for symmetric positive definite matrices,
- the Minimal Residual (MINRES) method for symmetric indefinite matrices,
- the Generalized Minimal Residual (GMRES) method for general matrices, and
- the Flexible Generalized Minimal Residual (FGMRES) method for non-stationary preconditioners.

It’s worth noting that our network, designed as a linear operator, can be effortlessly integrated into these two iterative frameworks.

2.2 Multigrid Algorithm

The multigrid algorithm, as described in Trottenberg et al. [40], is a category of solvers used for solving linear systems stemming from the discretization of partial differential equations (PDEs). This algorithm is characterized by its multilevel structure, where it performs a series of iterative processes across grids of different resolutions.

The efficient exchange of information in the multigrid algorithm is enabled by two crucial operators: the restriction operator and the prolongation operator. The restriction operator plays a key role in transferring the residual from a finer grid to a coarser one, effectively condensing the information. On the other hand, the prolongation operator is responsible for interpolating the solution from a coarser grid back to a finer grid. This dual mechanism ensures that while each level of the grid performs localized computations, their collective actions contribute to a global effect, enhancing the overall efficiency and accuracy of the algorithm.

To provide a clearer understanding, a classical two-grid algorithm is exemplified in Algorithm 1. This algorithm serves as a fundamental example of the multigrid method.

Algorithm 1 Two-grid method

- 1: Setup coarse grid operator A_c and transfer operators P and R .
 - 2: Compute the residual $r = rhs - Ax$ on the finest grid.
 - 3: Solve the correction equation $Ax = r$ on the finest grid by some simple iterative method.
 - 4: Restrict the residual r to a coarser grid r_c .
 - 5: Solve the correction equation $A_c x_c = r_c$ on the coarser grid by some iterative method.
 - 6: Interpolate the correction x_c from the coarser grid to the finest grid. Update the solution x on the finest grid.
 - 7: Do additional iterations on the finest grid.
-

The multigrid algorithm extends its functionality hierarchically by recursively applying the previously mentioned steps on progressively coarser grids. In the context of a linear equation, enhancing accuracy can be achieved via integrating it into iterative methods mentioned in Section 2.1.

Specifically, a classical geometric multigrid (GMG) method on a structured grid can be implemented as follows:

- Reduce the coarse grid size to the half of fine grid;
- Discretize the PDE on the coarse grid to set up the coarse grid operator A_c ;
- Use the bilinear interpolation to set up the prolongation operator P and restriction operator R ;
- Use the weighed-Jacobi method to solve the equation $Ax = r$ on each level.

This GMG method is straightforward to implement and efficient for many elliptic PDEs. However, its efficiency diminishes when applied to more complex problems, such as the convection-diffusion equation. We will use this method as a baseline for comparison with our learnable solver in the experiments.

2.3 Neural Network

Deep learning encompasses a diverse array of components with learnable parameters, among which CNNs are particularly notable. CNNs are a category of deep neural networks predominantly used for analyzing visual imagery and are characterized by their shift-invariant or space-invariant properties. In essence, a CNN performs a weighted summation over a local area of the input, applying this same convolutional kernel uniformly across all input regions. The size of the CNN’s output can either match or be smaller than the input, which is determined by the stride of the convolution. Mathematically, this operation can be represented as a matrix K multiplying a vector x ,

$$y = CNN(x) = Kx. \tag{2}$$

A transposed operation can be performed via a Transposed Convolutional Neural Network (TCNN) [41] on the input, i.e.,

$$y = TCNN(x) = K^T x. \tag{3}$$

Thus, a TCNN can be used to upscale the input. The combination of CNN and TCNN can emulate the prolongation operator and restriction operator in the multigrid algorithm. We further categorize CNN functionality as follows:

- reChannelCNN: It adjusts the input channels to match the output channels while keeping the input size unchanged.
- RCNN: Similar to the restriction operator in MG, it reduces the input size by half, i.e., $stride = 2$.

Except for RCNNs and TCNNs, all other CNNs will keep the input size unchanged in our experiments. For simplicity, we use the same symbol for the CNN kernel and its corresponding operator matrix. We use a 3x3 kernel for all CNNs and TCNNs and do not adjust the kernel size in our experiments. These two types of layers form the basic computational units of the proposed solver.

An important computation structure in deep learning is ResNet [1], which is a type of CNNs with a skip connection. It was designed to address the vanishing gradient problem in deep neural networks and aligns with numerous state update algorithms in numerical PDEs (i.e., Euler scheme for time-evolution PDEs). Mathematically, it can be expressed as:

$$y = ResNet(x) = Kx + x. \quad (4)$$

Such a layer can be stacked to form a deep neural network (5), as illustrated in Fig. 1. This skip connection concept is successfully used in our related works in their forms.

$$\mathbf{w} = ResNet_3(ResNet_2(ResNet_1(x))) \quad (5)$$

With restrict and prolongation operators, we can naturally form a ResNet network with a twogrid hierarchy

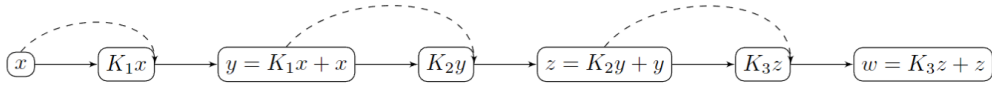


Figure 1: Stacked ResNets

(see Fig. 2). To extend the down and up cycle deeper we gain the multigrid structure of the proposed solver

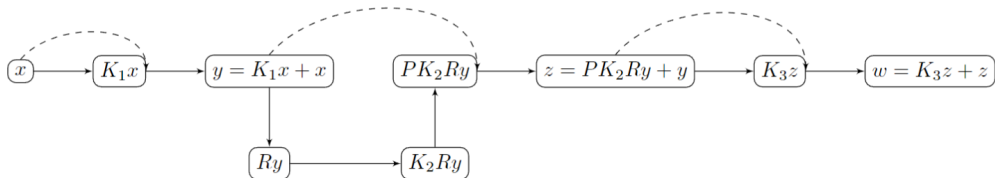


Figure 2: Stacked ResNets with twogrid hierarchy

(see Fig. 4, Alg. 3).

Despite those important networks and structures, another critical component for deep learning is the nonlinear activation function, which combines with the layered structure to form a nice universal approximator. It is a common practice to set nonlinear activation function σ after each CNN layer and add bias term b . The formula expression of the nonlinear ResNet is

$$y = NonLinearResNet(x) = \sigma(Kx + b) + x. \quad (6)$$

We will utilize it where nonlinearity is needed.

2.4 Discretization of PDEs on Structured Grids

CNNs can implement discretization of a linear PDE in a structured grid. Consider a two-dimensional convection-diffusion equation with heterogeneous diffusion coefficient and a fixed velocity \mathbf{v}

$$-\mu(x, y)(\partial_{xx}u(x, y) + \partial_{yy}u(x, y)) + \mathbf{v} \cdot \nabla u(x, y) = f(x, y), \quad (7)$$

As velocity is set as a constant vector, we use a normalized vector in this paper. The first-order upwind scheme [42] for this equation can be implemented with two CNNs, as follows:

$$K = \frac{1}{h} \left\{ \frac{1}{\mathbf{Re}} \begin{bmatrix} 0 & -1 & 0 \\ -1 & 4 & -1 \\ 0 & -1 & 0 \end{bmatrix} + \mathbf{v} \cdot K_{upwind} \right\}, \quad (8)$$

where h is the grid length, $\mathbf{Re} = h/\mu$ is the mesh Reynolds number [43], and K_{upwind} is the upwind scheme kernel. We use a bold symbol for \mathbf{Re} to distinguish with its range limit (see section 4.1). \mathbf{Re} measures the dominance of convection over diffusion, or the ratio of the unsymmetric part from an algebraic perspective. If we keep \mathbf{Re} unchanged for a larger grid, we are considering an equation with lower diffusion coefficient. This equation is often considered difficult to handle if \mathbf{Re} is significantly high [44, 45]. K_{upwind} is a weighted summation of several space-difference kernels below,

$$dx^+ = \begin{bmatrix} 0 & 0 & 0 \\ 0 & -1 & 1 \\ 0 & 0 & 0 \end{bmatrix}, \quad dx^- = \begin{bmatrix} 0 & 0 & 0 \\ -1 & 1 & 0 \\ 0 & 0 & 0 \end{bmatrix}, \quad dy^+ = \begin{bmatrix} 0 & 1 & 0 \\ 0 & -1 & 0 \\ 0 & 0 & 0 \end{bmatrix}, \quad dy^- = \begin{bmatrix} 0 & 0 & 0 \\ 0 & 1 & 0 \\ 0 & -1 & 0 \end{bmatrix} \quad (9)$$

Given velocity $\mathbf{v} = (v_x, v_y)$, we can define

$$v_x^+ = \max(v_x, 0), \quad v_x^- = \min(v_x, 0), \quad v_y^+ = \max(v_y, 0), \quad v_y^- = \min(v_y, 0) \quad (10)$$

and then the upwind scheme kernel can be written as

$$K_{upwind} = (v_x^+ dx^- + v_x^- dx^+, v_y^+ dy^- + v_y^- dy^+) \quad (11)$$

In this study, we only consider problems with zero Dirichlet boundary conditions on a two-dimensional rectangular domain. Correspondingly, we apply zero padding to CNNs when necessary on solve phase. Different padding strategies can be employed for various boundary conditions. It's worth noting that through discretization on the rectangular domain with a structured grid, each variable can form a tensor. During the learning process, we normalize the input by eliminating the factor $1/h$ for different problem sizes and refer to $coef = 1/\mathbf{Re} = \mu/h$ as the coefficient (tensor) for this discretized problem.

3 Methodology

Before we delve into the specifics of our approach, it's important to reiterate the three guiding principles that are fundamental to the design of our proposed solver:

- **P1.** Implement a multigrid hierarchical computation architecture for state updates;
- **P2.** Design the network to function linearly for the right-hand-side term of the equations;
- **P3.** Share weights across different levels within the multigrid hierarchy.

These principles are not only central to many classical multigrid algorithms but also serve as the cornerstone for our development of an end-to-end learnable solver.

Our proposed solver, inspired by the multigrid algorithm, operates in two distinct phases: the setup phase and the solve phase.

1. Setup Phase: This initial phase involves constructing the necessary information for each level of the multigrid hierarchy. This information lays the foundation for the subsequent solve phase. The setup is performed only once for a specific problem and is critical for preparing the solver for efficient operation.
2. Solve Phase: In this phase, we utilize the information prepared during the setup phase to sequentially update the state across different levels of the hierarchy. The solve phase is iterative, allowing for repeated execution until the solution reaches a satisfactory level of accuracy.

In the upcoming subsections, we'll delve into the intricacies of these two phases. We'll outline their design in detail and explain how they adhere to our three guiding principles. Additionally, we'll discuss the training aspects of our solver, providing insights into how the network is prepared to tackle PDE problems effectively.

3.1 Setup Phase

For this structured grid problem, we consider a similar strategy as GMG (see section 2.2) to setup the solver, which is to discretize the PDE on the coarser grid to form the coarse grid operator A_c . Our setup phase can be split into two steps:

- **Setup1.** use RCNN to restrict the problem coefficient tensor from fine grid to coarse grid
- **Setup2.** use multi-layered nonlinear ResNet to map those coefficient on each level into setup tensors needed for the solve phase.

The setup tensors, once computed, are stored and utilized in every iteration of the solve phase. Given that the setup phase is executed only once, the network in **Setup2** can be designed with sufficient layers to learn complex nonlinear mappings, and we choose four layers in use. Our experiments indicate that the \tanh activation function outperforms $ReLU$ for the chosen discretized problem. Consequently, we use \tanh after every CNN hidden layer in the ResNet of **Setup2**, the sole part where we aim to construct nonlinear mappings. Fig. 3 illustrates the setup computation framework, and Alg. 2 provides a detailed implementation.

Algorithm 2 Setup phase

```

1: procedure SETUP( $coef, level$ )
2:    $setup\_outs \leftarrow []$ 
3:    $coef \leftarrow reChannelCNN(coef)$ 
4:   for  $lv$  in  $1, 2, \dots, level$  do
5:      $setup\_outs.append(NonLinearResNet(coef))$ 
6:     if  $lv < level$  then
7:        $coef \leftarrow RCNN(coef)$ 
8:     end if
9:   end for
10:  return  $setup\_outs$ 
11: end procedure

```

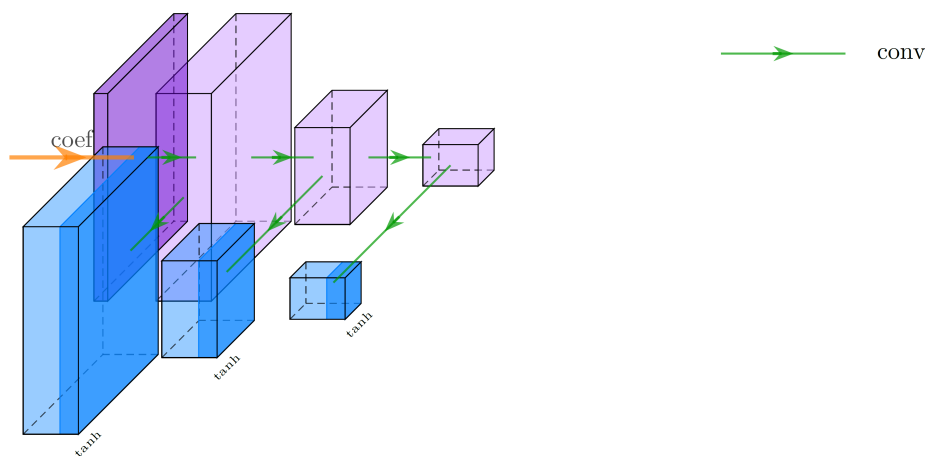


Figure 3: The 3-level setup network. The inner network (in pink) is used to restrict the problem coefficient tensor (in magenta) from fine to coarse grid. The outer network (in blue) maps those coefficient on each level into setup tensors needed for the solve phase. The right-banded blue boxes indicate the use of the \tanh activation function.

To use the same model for different levels, we share the corresponding weights of CNNs for the two multigrid hierarchies, i.e., following **P3**. An effect of weights sharing is the same number of channels over various levels.

Remark 3.1 (Setup phase input). *Not only problem coefficient but any tensor containing complete information used to discretize PDEs can be imported into the setup network. Therefore, when the discretization method is unknown and only matrix data is accessible, we can import matrix data as a tensor to the setup network. For example, if the matrix dataset is of the stencil form*

$$K = \begin{bmatrix} 0 & 0 & 0 \\ 0 & c_3 & c_2 \\ 0 & c_1 & 0 \end{bmatrix}, \quad (12)$$

where c_1, c_2, c_3 are probably different over the domain, we can import this matrix as coefficient tensor

$$\text{concat}(c_3, c_2, c_1), \quad (13)$$

to the setup network. This way, we can use the proposed setup network to learn the mapping from the matrix to setup tensors.

Remark 3.2 (Setup phase structure). *There might be lots of structure for the setup phase to explore without conflict with the three principles. Work [33] use a multigrid-like V-cycle and [34] goes through a down cycle. We have tried several and finally chose this one to mimic the process of the GMG setup phase. It works slightly better than others. Actually, we can see that there is no computation dependence on **Setup2** network, which is of potential high complexity. Therefore one can further optimize code to parallel this network. Though there is much flexibility, it works as the handler of the user’s matrix data and might be closely related to the final learning performance. We will leave further exploration of the impact of the setup phase structure to future work.*

3.2 Solve Phase

Solve phase is the central part of our design, reflecting all three principles. To comply with **P1**, we employ a multigrid-hierarchical extension of ResNet (as depicted in Fig. 2) to update the state. The specific implementation is detailed in Alg. 3. A 3-level network illustration is in the lower part of Fig. 4, with the setup output tensors displayed at the top, which we will discuss soon.

To adhere to **P2**, we avoid using any nonlinear activation function or bias in the solve phase. The challenge lies in leveraging the setup tensors while maintaining the network as a linear operator for the right-hand-side. We find that the simple **multiply** operation works well. This means that the input of a convolutional layer in *ResNetDown()* and *ResNetUp()* is multiplied with a setup tensor on each level, i.e.,

$$y = \text{ResNetDown}(\text{setup_out}, x) = \text{ResNet}(\text{setup_out} \times x), \quad (14)$$

$$y = \text{ResNetUp}(\text{setup_out}, x) = \text{ResNet}(\text{setup_out} \times x). \quad (15)$$

From a GMG perspective, we construct a smoother for each level based on its problem coefficient. Lastly, **P3** is easily obeyed by sharing weights. In other words, the functions *ResNetUp()*, *RCNN()*, *TCNN()*, and *ResNetDown* are the same across different levels.

The right-hand-side and the solver output are updated under a user-defined iteration framework. Those operations above form the entire landscape of the solve phase, and an illustration is in Fig. 4. Like the multigrid method, where the user can define the smoother sweeps on each level, we can also specify the number of *ResNet()* layers on each level. To minimize the serial computation of stacked ResNets, we use just one sweep on each level in our experiments.

Remark 3.3 (Status update strategy). *In the process of solving a linear system within a stationary iteration framework (refer to eq. 1), the solution update differs slightly from the status update of ResNet (see eq. 4). This difference lies in the participation of rhs in the update of x. During our initial research stage, we developed a multigrid-hierarchical extension that closely aligns with the stationary iteration algorithm. However, this approach did not significantly improve the results and introduced additional convolutional layers. Therefore, we opted for the simpler ResNet (refer to eq. 4) as the basis for the proposed solver structure.*

Algorithm 3 Solve phase

```

1: procedure SOLVE(setup_outs, rhs, level)
2:    $xs \leftarrow []$ 
3:    $x \leftarrow reChannelCNN(rhs)$ 
4:   for  $lv$  in  $1, 2, \dots, level$  do
5:      $x \leftarrow ResNetDown(setup\_outs[lv], x)$ 
6:     if  $lv < level$  then
7:        $xs.append(x)$ 
8:        $x \leftarrow RCNN(x)$ 
9:     end if
10:  end for
11:  for  $lv$  in  $level, level - 1, \dots, 1$  do
12:     $x \leftarrow ResNetUp(setup\_outs[lv], x)$ 
13:    if  $lv > 1$  then
14:       $x \leftarrow TCNN(x)$ 
15:       $x \leftarrow x + xs[lv - 1]$ 
16:    end if
17:  end for
18:   $x \leftarrow reChannelCNN(x)$ 
19:  return  $x$ 
20: end procedure

```

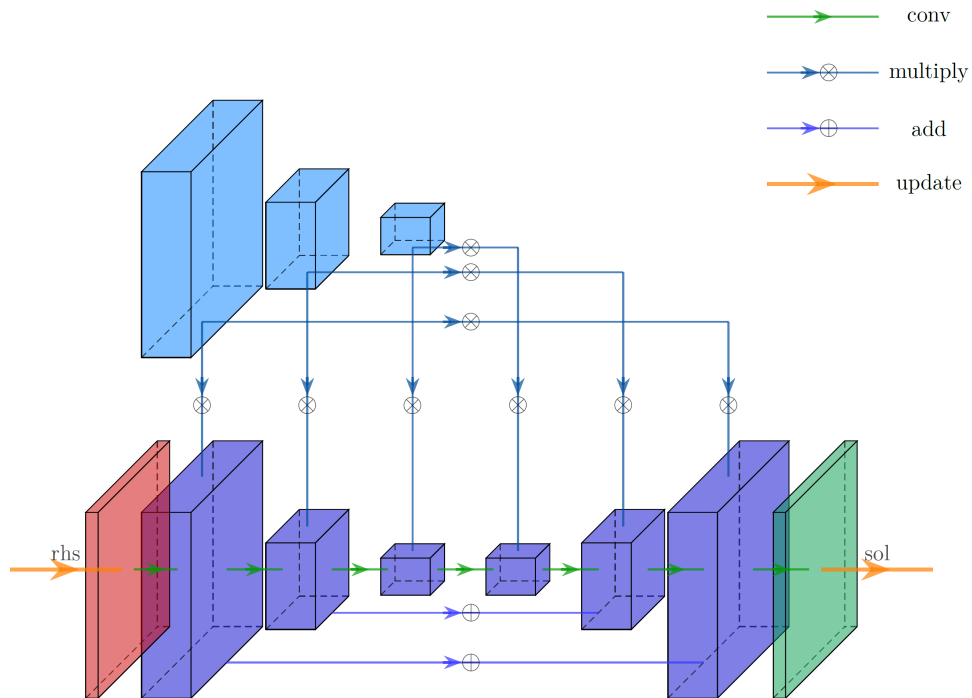


Figure 4: The 3-level solve network. The top part displays the setup output tensors (in blue). The bottom (in purple) represents the solve phase, where the right-hand-side and the solver output are updated under a user-defined iteration framework.

Remark 3.4 (Symmetric problem). Sometimes, the problem may have an inherent algebraic structure that the user wishes to preserve when setting up the solver. For example, for a symmetric problem, one could design a solver that operates as a symmetric operator and use the MINRES Krylov method to accelerate convergence. In our framework, we can enforce the network to be symmetric by sharing weights between `ResNetDown()` and `ResNetUp()`, and between `RCNN()` and `TCNN()`.

Remark 3.5 (Non-heterogeneous problem). We can simplify both the setup and solve phases for non-heterogeneous problems, where the problem coefficient remain constant. In these scenarios, we only need to generalize the solver over a range of one or several parameters. The space-invariant property of CNNs allows for direct use of the CNN layer, eliminating the need for our proposed additional multiply operation. Consequently, we can use a fully connected layer instead of a convolutional layer to handle the problem information. The output of the setup phase then becomes a column vector for each level, which can be set as the kernel of the convolutional layers in `ResNet()`. This approach coincides with the concept of meta-learning, a multi-task learning framework, as used in [32].

Remark 3.6 (Other multigrid patterns). The proposed structure represents just one of several options that adhere to our three guiding principles. Principle **P1** establishes the basic computation pattern. We can emulate other multigrid patterns, such as semi-coarsening, or incorporate add-type operations instead of multiply-type ones. These variations could offer additional benefits, similar to those observed in classical multigrid methods. Exploring these alternative structures for the solve phase remains a subject for future research.

Remark 3.7 (Vector-type PDEs). Our proposed solver can be naturally generalized to accommodate vector-type PDEs by simply adjusting the number of input and output channels. However, it does not support PDEs where different unknowns vary in size, as exemplified by the Marker-And-Cell (MAC) scheme for Stokes equations [46]. Addressing this limitation and extending the solver’s capabilities to handle such problems is a goal for our future research.

3.3 Training

The training of the proposed solver is minimizing the square of the residual norm of the linear equations, which is always taken as the convergence criterion of iterative methods. The loss function can be written as

$$L = \frac{1}{N} \sum_{i=1}^N \|rhs_i - A_i x_i\|^2 \quad (16)$$

where N is the number of data, rhs_i is the input (right-hand-side), x_i is the output (solver-guessed solution), and A_i is the discretized linear operator, which is decided by another input – coefficient tensor $coef_i$. Under the machine learning context, it is an unsupervised regression task, as we do not know the ground truth of the solution. Considering the frequency distribution of the white noise process is still white noise, which means it covers all ranges of frequency, we generate rhs_i as a white noise tensor. In practice, the coefficient tensor should be generated to fit one’s application scenarios and our generating method is describe in experiments section 4.1.

During training, We only perform one iteration of the solve phase for each coefficient tensor. The right-hand-side and coefficient are generated randomly for every batch. The whole training process, which combines the setup and solve networks, is illustrated in Fig. 5.

Remark 3.8 (Supervised learning strategy). We could also employ a supervised learning pattern through the following steps:

1. Generate a random tensor as the ground truth solution sol_i .
2. Use $A_i sol_i$ as the right-hand-side, i.e., rhs_i sent to the solver.

In this case, we can define the loss function as the square of the error norm:

$$L = \frac{1}{N} \sum_{i=1}^N \|x_i - sol_i\|^2 \quad (17)$$

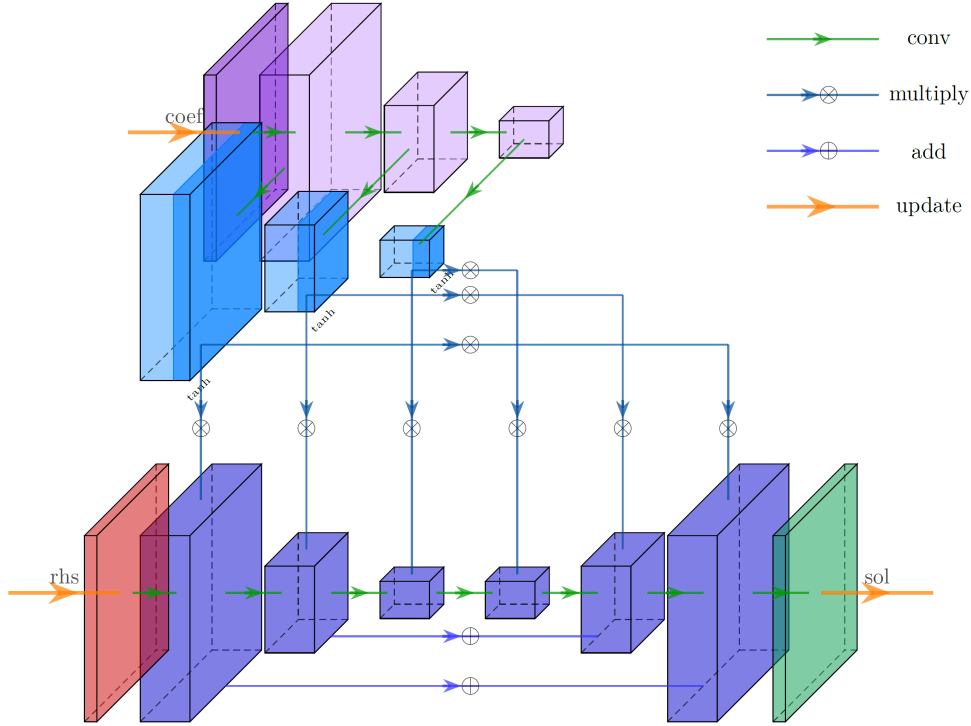


Figure 5: The 3 level training network. A combination of setup and solve networks. The right-hand-side, coefficient and solver output are updated in every training batch.

However, generating a suitable sol_i might be questionable. Mathematically, the right-hand-side function usually has weak smoothness and only needs to be of L_2 regularity, while the solution function is usually of strong smoothness and needs to be of, for instance, H^1 regularity or even H_0^1 . Therefore, it is not straightforward to generate a suitable sol_i for a given A_i . In our experiments, we find that the unsupervised learning pattern works well and does not gain benefit from the supervised learning pattern.

Remark 3.9 (Data distribution of right-hand-side). *The linear nature of the solve network, in its interaction with the right-hand-side (RHS) term, is a pivotal aspect of both the solve phase and the training process. The efficacy of deep learning is closely linked to the distribution of input data. Training a solver to achieve high accuracy after just a single application can be challenging, even only for a fixed RHS distribution. Typically, higher accuracy in linear equations is attained through an iterative method, leading to an updated RHS within a possibly new distribution. This creates a need for generating the appropriate RHS distribution during the solve phase, as seen in previous works [33, 34]. In our approach, we leverage the linear property of the network to enhance its generalization ability. This is crucial because training data, when linearly combined, can span a much broader data space. Training on a white noise dataset proves to be adequate due to this property. Our commitment to minimizing the reliance on expert knowledge and upholding the linear characteristic of the solver forms a fundamental part of our strategy. This approach not only simplifies the training process but also expands the potential applicability and robustness of the learned solver.*

4 Experiments

4.1 Basic Settings

Our experiments were conducted on a V100 GPU with 16GB memory, using PyTorch [47] as our deep learning framework. The code is available at <https://gitee.com/xiehuohuo77/heteromgcnm.git> (open

after publication). The GMG method, also implemented in PyTorch, is used as a comparison, representing a classical method with a similar computation pattern.

Problem settings. We trained the solver to solve the convection-diffusion equation with heterogeneous diffusion coefficient (see section 2.4). The convection-diffusion equation has fixed velocity $v = (\sin(0.5), \cos(0.5))$ over the domain. In this experiment, we generate $coef$ from a given random tensor to range $[\epsilon, 1], 0 < \epsilon < 1$ via two steps

1. firstly linearly map the random tensor to range $[0, -\log_{10}(\epsilon)]$ as $random_power$
2. then map the tensor to range $[\epsilon, 1]$ via $10^{-random_power}$

The random tensor is generated as white noise or from other distributions, which we will introduce to discuss the data distribution dependence issue in the experiment section 4.3. Recall that $\mathbf{Re} = 1/coef$, therefore the range of \mathbf{Re} is $[1, 1/\epsilon]$. For simplicity, we use the non-bold symbol Re to denote the range limit of \mathbf{Re} , i.e., $\mathbf{Re} \in [1, Re]$. Unless otherwise specified, we use $Re = 1000$ in our experiments.

Iterative method settings. In our experimental setup, each iteration result is replicated ten times using randomly selected coefficients. The right-hand-side (RHS) for these tests is set as a constant, $\mathbf{1}$, which notably is not part of the training dataset for the RHS. Although it’s common to employ the Krylov method, particularly the Generalized Minimal Residual (GMRES) method, to accelerate convergence in iterative methods, we found that GMRES only marginally reduces the number of iterations for both our proposed solvers and the Geometric Multigrid (GMG) method in this specific problem. Interestingly, this marginal reduction in iterations actually leads to increased total computation time. Given this observation, we decided against using the Krylov method in our experiments. Instead, we opted for stationary iterations for all tested methods. For assessing convergence, we set the criterion to be the relative residual norm, with a tolerance threshold of 1E-8 for double precision computations. This approach ensures a consistent and fair comparison across different methods under test.

MGCNN settings. We gradually train the solver from minor to larger sizes, simultaneously reducing the batch sizes. The training process covers grids of sizes 31×31 , 63×63 , 127×127 , 255×255 , and 511×511 . We provide the details of the training settings in Appendix A.1. We tested all solvers over grids ranging from 31×31 to 4095×4095 , the maximum size our GPU memory can accommodate. The main hyperparameter of the proposed solver is $level$, $sweeps$ and ($hidden$) $channels$. We found that the reduction of $level$ significantly deteriorates convergence, and one sweep is enough to reach satisfactory convergence. Therefore, we fix $sweeps = 1$ and use $level = 4, 5, 6, \dots$ with respect to $grid_size = 31, 63, 255, \dots$ for below experiments of the proposed solver. If not specified, we use $channels = 8$ for the proposed solver.

GMG settings. We manually tune the GMG parameters to improve its results. We set $weight = 0.67$ and perform three $sweeps$ for the weighed-Jacobi smoother, and use $level = 2, 3, 4, \dots$ corresponding to $grid_size = 31, 63, 255, \dots$ for the comparisons below. This setting of $level$ is smaller than the proposed solvers, as GMG does not gain benefit from more levels as the proposed solvers does.

Remark 4.1 (Training time). *The multilevel training strategy is time-efficient, taking no more than 2.5 hours on double precision. Training on single precision can be even faster, taking no more than 20 minutes. However, this results in some loss of convergence performance, especially for large grid sizes. Therefore, we only present the outcomes of the solver trained in double precision here.*

In the upcoming subsections, we will explore the impact of hyperparameter **hidden channels** in section 4.2. Subsequently, we aim to investigate its dependence on coefficient data distribution in section 4.3, including the impact of **distribution range** and **distribution pattern**.

4.2 Impact of Channels

Our focus is the impact of $channels$ on the solver. Specifically, we select $channels = 4, 8, 12$ and present the iteration number and consumed time results in Table 1 and 2. Here, we also conduct tests on float computation, using 1E-4 as the convergence tolerance. However, solvers can only reach a 1E-3 tolerance for the 4095×4095 grid, so we only present results for grids from 31×31 to 2047×2047 for the float computation. We can see that the proposed solver performs better than GMG in both precision in the solve phase. However, GMG almost takes no time in the setup phase, while the proposed solver takes a higher cost setup phase.

Considering that the setup phase is only executed once, and its time cost is much smaller than the iterative solve phase, it is acceptable.

| float, 1E-4 | channel4 | | | channel8 | | | channel12 | | | GMG | | |
|-------------|----------|-------|-------|----------|-------|-------|-----------|-------|-------|-------|-------|-------|
| grid | iters | setup | solve | iters | setup | solve | iters | setup | solve | iters | setup | solve |
| 31x31 | 5.7 | 2.6 | 9.6 | 4 | 2.4 | 6.8 | 4 | 2.0 | 5.6 | 10 | 1.9 | 39.4 |
| 63x63 | 6 | 2.9 | 10.9 | 4 | 2.6 | 6.8 | 4 | 2.6 | 6.6 | 11.3 | 2.4 | 53.8 |
| 127x127 | 6 | 3.1 | 11.3 | 4 | 2.8 | 7.0 | 4 | 3.0 | 7.2 | 13 | 2.7 | 68.0 |
| 255x255 | 7 | 3.8 | 15.9 | 4.8 | 3.6 | 10.4 | 4 | 3.8 | 9.0 | 15 | 3.7 | 105.9 |
| 511x511 | 9 | 4.4 | 23.6 | 5 | 4.0 | 13.6 | 5 | 4.4 | 15.3 | 18 | 4.5 | 150.4 |
| 1023x1023 | 13 | 5.1 | 49.6 | 7 | 5.4 | 32.6 | 5 | 7.3 | 29.7 | 24 | 5.2 | 244.3 |
| 2047x2047 | 18 | 10.8 | 168.9 | 9 | 17.9 | 135.2 | 6 | 26.0 | 126.6 | 34 | 6.2 | 555.7 |

Table 1: Impact of channels on the Solver (float precision, convergence tolerance is 1E-4), iters: iteration number, setup: setup time(ms), solve: solve time(ms)

| double, 1E-8 | channel4 | | | channel8 | | | channel12 | | | GMG | | |
|--------------|----------|-------|-------|----------|-------|-------|-----------|-------|-------|-------|-------|--------|
| grid | iters | setup | solve | iters | setup | solve | iters | setup | solve | iters | setup | solve |
| 31x31 | 11 | 1.7 | 12.3 | 7 | 2.1 | 9.1 | 7.2 | 2.3 | 10.7 | 16.7 | 1.5 | 50.9 |
| 63x63 | 12 | 1.7 | 13.1 | 7.1 | 2.3 | 10.5 | 7.1 | 2.6 | 11.7 | 19.2 | 2.0 | 74.8 |
| 127x127 | 12 | 2.0 | 15.2 | 8 | 2.8 | 14.4 | 7 | 3.0 | 14.2 | 21 | 2.7 | 104.5 |
| 255x255 | 13 | 3.8 | 20.9 | 8 | 3.5 | 18.9 | 7.5 | 3.8 | 20.1 | 25.9 | 3.7 | 173.8 |
| 511x511 | 17 | 2.8 | 42.0 | 9 | 4.1 | 33.6 | 8 | 4.7 | 36.5 | 33.7 | 4.5 | 266.2 |
| 1023x1023 | 23 | 6.6 | 152.1 | 12 | 10.8 | 123.0 | 9 | 15.5 | 122.3 | 45 | 5.4 | 533.6 |
| 2047x2047 | 30 | 24.4 | 687.0 | 15 | 40.6 | 536.6 | 12 | 58.8 | 592.7 | 61 | 5.9 | 2066.8 |
| 4095x4095 | 43 | 96.6 | 3.6E3 | 22 | 161.6 | 3.1E3 | 15 | 234.5 | 3.2E3 | 84 | 8.0 | 1.1E4 |

Table 2: Impact of channels on the Solver (double precision, convergence tolerance is 1E-8), iters: iteration number, setup: setup time(ms), solve: solve time(ms)

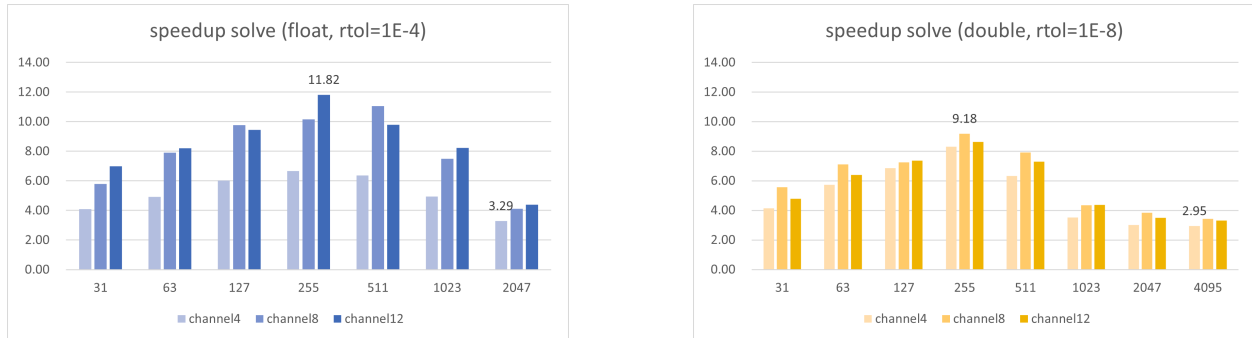


Figure 6: Time speedup of our trained solver over the GMG method in the solve phase.

The speedup of the proposed solver over the GMG method in solve phase is shown in Fig. 6, and the speedup for total time is shown in Fig. 7. In the iterative solve phase, our trained solvers achieve a speedup of around 3x to 10x for the three tested channel numbers on both float and double computation. Considering the total time, the speedup is about 3x to 8x, which is also desirable. The highest speedup occurs on medium grid sizes, where the iterations of our trained solver do not increase much, and the GPU computation time is not sensitive to the number of channels. In float precision, the GPU is even less susceptible to such an increase in computation complexity, achieving a higher speedup than double precision. We should remember that GMG involves three sweeps of the smoother (see section 4.1). Therefore, the speedup of our trained

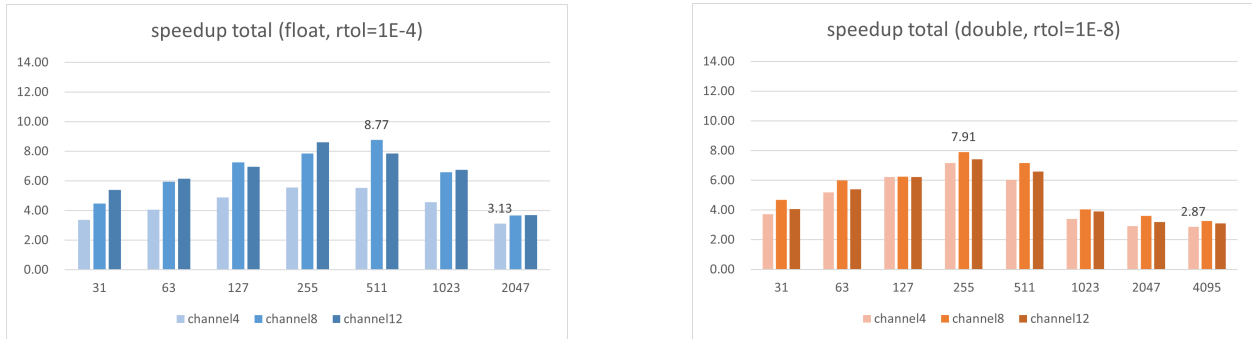


Figure 7: Time speedup of our trained solver over the GMG method in total.

solver mainly stems from the reduction in the number of iterations, owing to the high number of channels and the excellent learning ability of deep neural networks.

Remark 4.2 (Subspace update view). *If we examine the update method in the solve phase (see section 3.2), we can see that the main difference from traditional algorithms is the number of channels. The proposed solver updates several channels of state simultaneously, which can be viewed as updating a subspace rather than one direction. The convergence of such a subspace method is unknown for now, and we leave it for future work.*

4.3 Dependence on Data Distribution of Coefficient

Deep learning performance is widely acknowledged to be intricately linked to input data distribution. In this subsection, we delve into the influence of both the coefficient distribution range and pattern on the convergence behavior of our trained solver. For simplicity, we borrow terminology from machine learning, referring to our tests as "transfer tests." It's important to note that, unlike traditional transfer learning, no re-tuning is performed during these tests. The results of the GMG solver for comparison are available in Appendix A.2.

We generate the coefficient tensor from a random tensor with a specified distribution range (refer to Section 4.1). In addition to white noise, we employ the following distributions for generating the random tensor:

- **CIFAR10** [48]: A dataset comprising 60,000 32x32 color images across 10 classes. We utilize the first channel of the images to generate the random tensor.
- **FMNIST** [49]: A dataset of 60,000 28x28 grayscale images representing 10 fashion categories.
- **MNIST** [50]: A dataset of 70,000 28x28 grayscale images depicting the digits 0 through 9.
- **mldata**: Random tensors generated using a multi-level random data generation method. Details of our proposed method are outlined in Appendix A.4.

The first three datasets comprise real-world images. To adapt them to our experiment, we interpolate the randomly selected images to the desired grid size. Additionally, we design a multi-level data generation method to create **mldata** for the transfer tests. We also generate the coefficient tensor from white noise with different distribution ranges, namely $Re = 10$ and $Re = 10^5$. The proposed solver is exclusively trained on coefficients from white noise with $Re = 1000$, and its convergence is tested on the aforementioned distributions. The number of iterations is summarized in Table 3. We observe that the performance remains reliable for ranges $Re = 10$, $Re = 10^5$, and datasets CIFAR10, **mldata**. However, it degrades significantly for other datasets, especially on large grid sizes.

To address the distribution transfer issue, we train the solver with a mixture of white noise and CIFAR10 and test its convergence on the same distributions above. The corresponding iteration numbers are listed in Table 4. We observe that it performs almost equally well on different distribution range limits and distribution patterns. It only slightly increases the number of iterations on originally trained white noise with $Re = 1000$.

| grid | noise | CIFAR10 | FMNIST | MNIST | mldata | Re10 | Re10 ⁵ |
|-----------|-------|---------|--------|-------|--------|------|-------------------|
| 31x31 | 7 | 8.2 | 13.6 | 15.1 | 7.7 | 8.1 | 7 |
| 63x63 | 7.1 | 9.8 | 17.3 | 18.4 | 8.1 | 9 | 7.8 |
| 127x127 | 8 | 11.5 | 19.2 | 19.6 | 9.3 | 9 | 8 |
| 255x255 | 8 | 11.1 | 20.6 | 20.9 | 10.5 | 10 | 8 |
| 511x511 | 9 | 13.4 | 22.5 | 24 | 11.8 | 12 | 9.9 |
| 1023x1023 | 12 | 15.9 | 25.2 | 31 | 13.8 | 15 | 12 |
| 2047x2047 | 15 | 19.3 | 39.7 | 45.2 | 16.9 | 21 | 16 |
| 4095x4095 | 22 | 25.1 | 62.3 | 105.8 | 23.2 | 31.7 | 22 |

Table 3: Iteration number of our trained solver over different coefficient distributions. Re10 and Re10⁵ refer to $Re = 10, 10^5$ with coefficients generated from white noise. The solver is trained only on coefficients from white noise with $Re = 1000$

| grid | noise | CIFAR10 | FMNIST | MNIST | mldata | Re10 | Re10 ⁵ |
|-----------|-------|---------|--------|-------|--------|------|-------------------|
| 31x31 | 7.1 | 7.6 | 9.8 | 10.0 | 7.3 | 7.6 | 7 |
| 63x63 | 7.1 | 7.9 | 9.7 | 10 | 7.5 | 7.1 | 7 |
| 127x127 | 7.2 | 8 | 9.7 | 9.6 | 8 | 7.6 | 7.6 |
| 255x255 | 8 | 8 | 9.5 | 9 | 8 | 8 | 8 |
| 511x511 | 10 | 9.6 | 9.6 | 9 | 9.8 | 8 | 10 |
| 1023x1023 | 12 | 12.4 | 11.7 | 10.1 | 12.6 | 10 | 13 |
| 2047x2047 | 16 | 15.9 | 13.6 | 12.7 | 16.6 | 13 | 17 |
| 4095x4095 | 22 | 22.3 | 19.9 | 17.1 | 22.4 | 17 | 23 |

Table 4: Iteration number of our trained solver over different coefficient distributions. Re10 and Re10⁵ refer to $Re = 10, 10^5$ with coefficients generated from white noise. The solver is trained on coefficient from a mixture of white noise and CIFAR10.

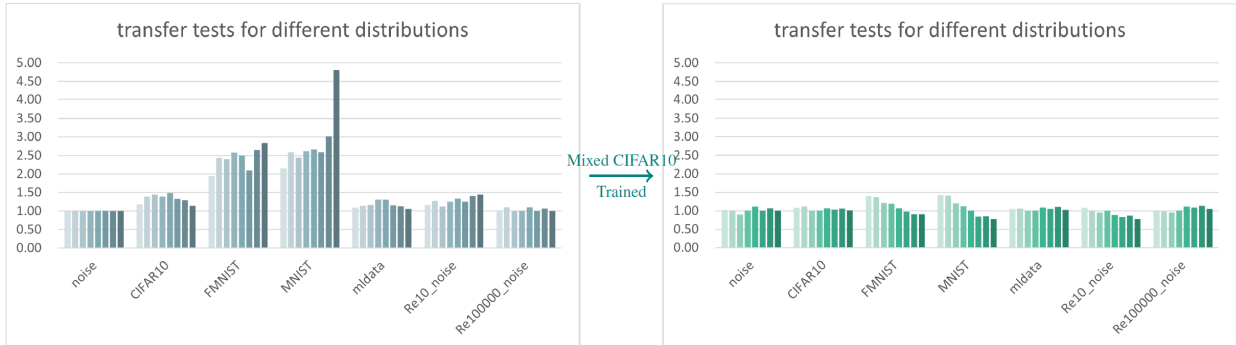


Figure 8: Ratio of iteration numbers of the proposed solver tested on different coefficient distributions over that of white noise. Deeper colors represent larger grid sizes. The left shows results when trained only with white noise, while the right depicts results when trained with a mixture of white noise and CIFAR10.

To clarify, we refer to the solver trained solely with white noise as the white-noise-trained Solver. Conversely, the solver trained on a coefficient dataset from a mixture of white noise and CIFAR10 is termed the mixed-CIFAR10-trained solver. The enhancement achieved by the mixed-CIFAR10-trained solver in transfer tests is clearly depicted in Fig. 8. In this figure, the number of iterations of the solver, when both trained and tested with white noise, is used as a reference point. The ratios of the number of iterations are computed for both the white-noise-trained Solver (left) and the mixed-CIFAR10-trained solver (right), each tested on a variety of data distributions. All ratios are reduced to around or even below 1.0, indicating enhanced robustness. For additional detailed results, including the \log_{10} of the coefficient tensors and convergence history of the the mixed-CIFAR10-trained solver, refer to Appendix A.3.

In summary, our proposed solver’s performance exhibits a dependence on the distribution of coefficient data and showcases reliable generalization across some untrained distributions. To enhance its robustness, we introduce a mixed training approach, combining white noise and CIFAR10. The mixed-CIFAR10-trained solver demonstrates consistent performance across different distribution range limits and patterns, with only a slight decline of convergence for the originally trained white noise with $Re = 1000$. These findings imply that practitioners should analyze the problem at hand and select a suitable distribution for training. Given the rapid training speed 4.1, training multiple parameters of a solver for different coefficient distributions and loading the appropriate one when using becomes a feasible strategy. Alternatively, training the solver on a mixture of several distributions can further enhance its robustness. Users can now focus on providing the data distribution, relieving them from the intricacies of designing a solver for a given problem.

5 Conclusion and Future Work

This research presents an innovative deep learning-based solver designed for linear partial differential equations (PDEs) discretized on structured grids. The solver is built on three key principles: (1) employing a multigrid computational structure, (2) applying the solver linearly to the right-hand-side, and (3) sharing weights across different levels. These principles collectively ensure fast convergence, excellent scalability, and broad applicability. The multigrid framework enhances the solver’s speed and adaptability to large problems. Its linear operation allows for seamless integration into various iterative methods and simplifies the training process (refer to Remark 3.9). Weight sharing across levels enables the solver to adapt to different problem sizes, and makes training more efficient in terms of both time and memory.

In our study, the solver effectively handles a convection-diffusion equation with varying diffusion coefficients, without requiring specialized domain knowledge. We explore the influence of hidden channels within the solver, noting their positive impact on convergence. Due to the GPU’s resilience to increased channels, particularly in small to medium problem sizes, our solver achieves about 3 to 8 faster performance than the GMG method under stringent accuracy demands. Additionally, we assess the solver’s performance with different data distributions for coefficients, finding reliable performance even with untrained distributions and varied range. A mixed coefficient dataset combining white noise and CIFAR10 data enhances robustness across distributions.

This work marks our initial foray into leveraging AI for solving PDEs. Its straightforward deployment and rapid convergence position it as a promising tool for linear PDE problems. Despite the progress detailed in previous sections, further research is necessary. Future directions include extending the principles to linear equations on unstructured grids, developing AI-based solvers for nonlinear equations, and addressing the inherent space-invariance of CNNs, which is suboptimal for heterogeneous problems and may lead to time-inefficient computation. We eagerly anticipate continuing our work in this dynamic and evolving field.

Acknowledgments

This research was supported in part by the National Key R&D Program of China grant 2020YFA0711904, the National Science Foundation of China grant 11971472.

A Appendix

A.1 Training Settings

Although training in this paper does not rigorously follow the dataset concept, we still use the terminology of epoch to control the training process, and the network will go through 1000 batches for each epoch. We train the solver from small to larger sizes gradually. The maximum batch size is 16 for the smallest size 31×31 and reduced to half for every double size until the minimum batch size, 2. The training process is done on 31×31 , 63×63 , 127×127 , 255×255 and 511×511 grid. The training parameter settings are shown in Table 5. Additionally, we pose the loss-decreasing history of the proposed solver in Fig. 9. According to the

| Parameter | Value | Description |
|----------------|-------|--|
| epochs | 50 | – |
| num | 1000 | number of batches in one epoch |
| lr | 0.003 | initial learning rate |
| optimizer | Adam | step_size = 2, gamma=0.8 |
| size_step | 10 | change data_size, level, batch_size every size_step |
| size | 31 | initial data size, double sizes every size_step |
| level | 4 | initial level, increase 1 every size_step |
| batch_size | 16 | initial batch size, reduce to its half every size_step |
| max_size | 511 | maximum data size |
| min_batch_size | 2 | maximum batch size |

Table 5: Training settings

training settings, the trained grid size changes for every 10,000 batches, and we can see a slight loss increase after each change.

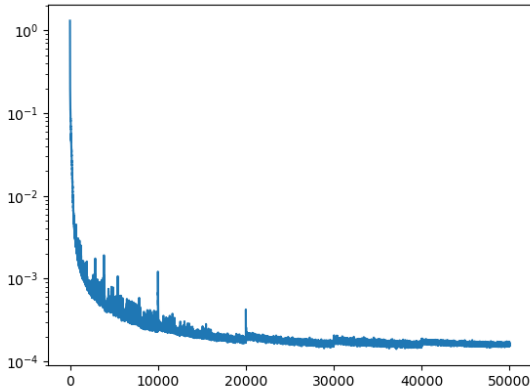


Figure 9: Loss decreases over training batches.

A.2 GMG Performance over Different Coefficient Distribution

As comparisons, we also test the GMG solver over different coefficient distributions and list the number of iterations in Table 6.

| grid | noise | CIFAR10 | FMNIST | MNIST | mldata | Re10 | Re10 ⁵ |
|-----------|-------|---------|--------|-------|--------|------|-------------------|
| 31x31 | 16.7 | 13 | 16.3 | 19.1 | 13 | 17.6 | 15 |
| 63x63 | 19.2 | 15.1 | 16.8 | 18.1 | 15 | 20 | 17.9 |
| 127x127 | 21 | 19.8 | 19.5 | 19 | 20 | 21 | 20 |
| 255x255 | 25.9 | 25.9 | 24.1 | 23.6 | 26.1 | 24.7 | 26 |
| 511x511 | 33.7 | 34.3 | 31.9 | 29.4 | 35.4 | 31 | 34.1 |
| 1023x1023 | 45 | 46.3 | 41.8 | 37.4 | 48 | 40 | 46 |
| 2047x2047 | 61 | 61.3 | 51.1 | 48 | 65.4 | 53 | 63 |
| 4095x4095 | 84 | 85.8 | 71.7 | 61.7 | 87.2 | 71 | 87 |

Table 6: The number of iterations of the GMG solver over different coefficient distributions.

A.3 Different Coefficient Distributions and Convergence History of the Proposed Solver

To give a glimpse of different coefficient distributions, we show the \log_{10} scale of coefficient tensors and convergence history of our mixed-CIFAR10-trained solver in Fig. 10. Table 4 in section 4.3 shows a detailed comparison of the proposed solver over different coefficient distributions.

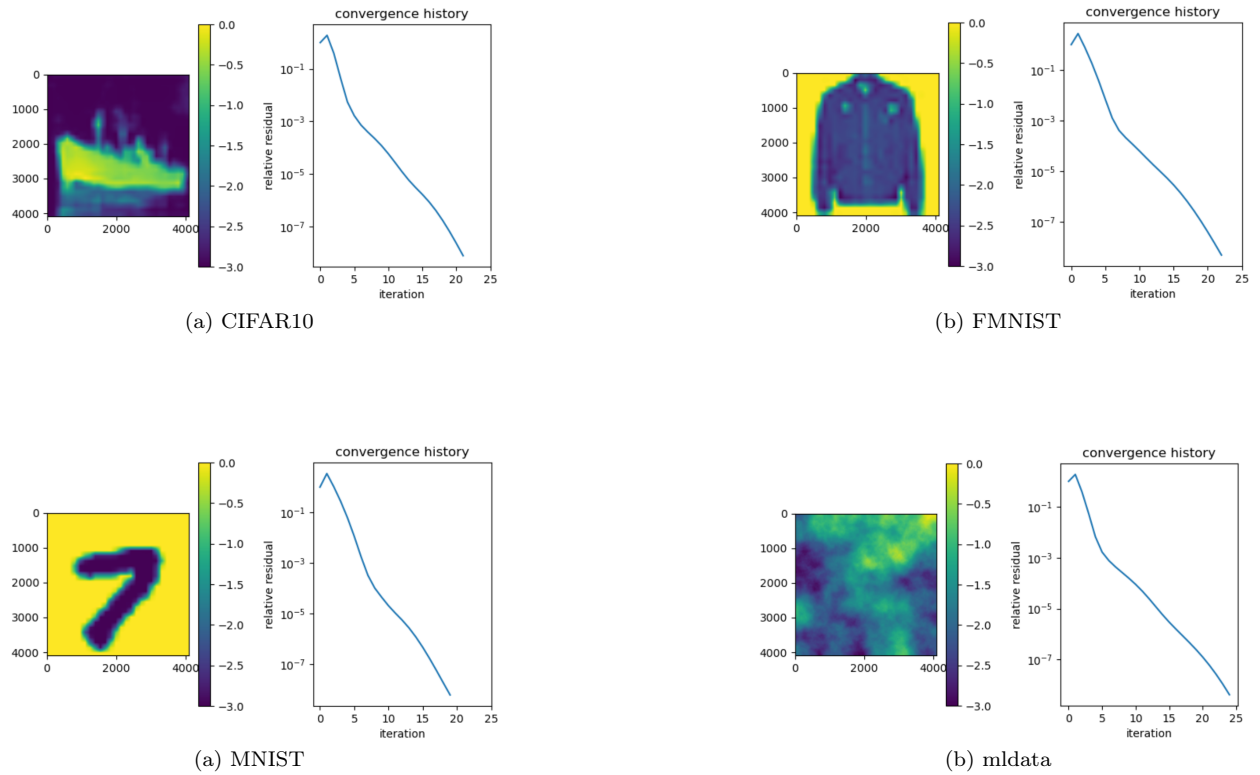


Figure 10: The \log_{10} scale coefficient tensor and convergence history. The proposed solver is trained over the mixed coefficient dataset, a combination of white noise and CIFAR10. The right-hand-side is constant, $\mathbf{1}$, and the grid size is 4095×4095 , both of which are not used at training.

A.4 Algorithm of Generating Multi-Level Data

Despite the white noise distribution and authentic world images, we design a multi-level data generation algorithm to test the impact of data distribution. Basically, we start from a small white noise tensor,

interpolate it to a larger size, and add some white noise to it. We repeat this process and interpolate it to the desired final size. The detailed algorithm is shown in Alg. 4. In our experiments, we set *init_size* as 5.

Algorithm 4 Generate Multi-Level Data

```
1: procedure GEN_DATA_MULTI_LEVEL(goal_size, levels, init_size)
2:   data  $\leftarrow$  white_noise(init_size)
3:   for i in 1, 2, ..., levels do
4:     data  $\leftarrow$  interpolate to size =  $2 \times$  data.size
5:     noise_ratio  $\leftarrow 2^{-i}$ 
6:     data  $\leftarrow$  data + noise_ratio  $\times$  white_noise(data.size)
7:   end for
8:   data  $\leftarrow$  interpolate to size = goal_size
9: end procedure
```

References

- [1] Kaiming He, Xiangyu Zhang, Shaoqing Ren, and Jian Sun. Deep residual learning for image recognition. In *Proceedings of the IEEE conference on computer vision and pattern recognition*, pages 770–778, 2016.
- [2] Ashish Vaswani, Noam Shazeer, Niki Parmar, Jakob Uszkoreit, Llion Jones, Aidan N Gomez, Łukasz Kaiser, and Illia Polosukhin. Attention is all you need. *Advances in neural information processing systems*, 30, 2017.
- [3] Ian Goodfellow, Jean Pouget-Abadie, Mehdi Mirza, Bing Xu, David Warde-Farley, Sherjil Ozair, Aaron Courville, and Yoshua Bengio. Generative adversarial nets. *Advances in neural information processing systems*, 27, 2014.
- [4] Tomas Mikolov, Ilya Sutskever, Kai Chen, Greg S Corrado, and Jeff Dean. Distributed representations of words and phrases and their compositionality. *Advances in neural information processing systems*, 26, 2013.
- [5] Tom Brown, Benjamin Mann, Nick Ryder, Melanie Subbiah, Jared D Kaplan, Prafulla Dhariwal, Arvind Neelakantan, Pranav Shyam, Girish Sastry, Amanda Askell, et al. Language models are few-shot learners. *Advances in neural information processing systems*, 33:1877–1901, 2020.
- [6] Jacob Devlin Ming-Wei Chang Kenton and Lee Kristina Toutanova. Bert: Pre-training of deep bidirectional transformers for language understanding. In *Proceedings of naacL-HLT*, volume 1, page 2, 2019.
- [7] Babak Alipanahi, Andrew Delong, Matthew T Weirauch, and Brendan J Frey. Predicting the sequence specificities of dna-and rna-binding proteins by deep learning. *Nature biotechnology*, 33(8):831–838, 2015.
- [8] John Jumper, Richard Evans, Alexander Pritzel, Tim Green, Michael Figurnov, Olaf Ronneberger, Kathryn Tunyasuvunakool, Russ Bates, Augustin Žídek, Anna Potapenko, et al. Highly accurate protein structure prediction with alphafold. *Nature*, 596(7873):583–589, 2021.
- [9] Vladimir Gligorijević, P Douglas Renfrew, Tomasz Kosciolk, Julia Koehler Leman, Daniel Berenberg, Tommi Vatanen, Chris Chandler, Bryn C Taylor, Ian M Fisk, Hera Vlamakis, et al. Structure-based protein function prediction using graph convolutional networks. *Nature communications*, 12(1):3168, 2021.
- [10] Deep Ray and Jan S Hesthaven. Detecting troubled-cells on two-dimensional unstructured grids using a neural network. *Journal of Computational Physics*, 397:108845, 2019.

- [11] Niccolo Discacciati, Jan S Hesthaven, and Deep Ray. Controlling oscillations in high-order discontinuous galerkin schemes using artificial viscosity tuned by neural networks. *Journal of Computational Physics*, 409:109304, 2020.
- [12] Alexandr Katrutsa, Talgat Daulbaev, and Ivan Oseledets. Deep multigrid: learning prolongation and restriction matrices. *arXiv preprint arXiv:1711.03825*, 2017.
- [13] Daniel Greenfeld, Meirav Galun, Ronen Basri, Irad Yavneh, and Ron Kimmel. Learning to optimize multigrid pde solvers. In *International Conference on Machine Learning*, pages 2415–2423. PMLR, 2019.
- [14] Jianguo Huang, Haoqin Wang, and Haizhao Yang. Int-deep: A deep learning initialized iterative method for nonlinear problems. *Journal of computational physics*, 419:109675, 2020.
- [15] Maziar Raissi, Paris Perdikaris, and George E Karniadakis. Physics-informed neural networks: A deep learning framework for solving forward and inverse problems involving nonlinear partial differential equations. *Journal of Computational physics*, 378:686–707, 2019.
- [16] Leah Bar and Nir Sochen. Strong solutions for PDE-based tomography by unsupervised learning. *SIAM Journal on Imaging Sciences*, 14(1):128–155, 2021.
- [17] Ben Moseley, Andrew Markham, and Tarje Nissen-Meyer. Solving the wave equation with physics-informed deep learning. *arXiv preprint arXiv:2006.11894*, 2020.
- [18] Chao Song, Tariq Alkhalifah, and Umair Bin Waheed. A versatile framework to solve the Helmholtz equation using physics-informed neural networks. *Geophysical Journal International*, 228(3):1750–1762, 2022.
- [19] Antonio Stanzola, Simon R Arridge, Ben T Cox, and Bradley E Treeby. A Helmholtz equation solver using unsupervised learning: Application to transcranial ultrasound. *Journal of Computational Physics*, 441:110430, 2021.
- [20] Bing Yu et al. The deep ritz method: a deep learning-based numerical algorithm for solving variational problems. *Communications in Mathematics and Statistics*, 6(1):1–12, 2018.
- [21] Lu Lu, Xuhui Meng, Zhiping Mao, and George Em Karniadakis. Deepxde: A deep learning library for solving differential equations. *SIAM review*, 63(1):208–228, 2021.
- [22] Georgios Kissas, Jacob H Seidman, Leonardo Ferreira Guilhoto, Victor M Preciado, George J Pappas, and Paris Perdikaris. Learning operators with coupled attention. *The Journal of Machine Learning Research*, 23(1):9636–9698, 2022.
- [23] Lu Lu, Pengzhan Jin, Guofei Pang, Zhongqiang Zhang, and George Em Karniadakis. Learning nonlinear operators via DeepONet based on the universal approximation theorem of operators. *Nature machine intelligence*, 3(3):218–229, 2021.
- [24] Ravi G Patel, Nathaniel A Trask, Mitchell A Wood, and Eric C Cyr. A physics-informed operator regression framework for extracting data-driven continuum models. *Computer Methods in Applied Mechanics and Engineering*, 373:113500, 2021.
- [25] Peter R Wiecha and Otto L Muskens. Deep learning meets nanophotonics: a generalized accurate predictor for near fields and far fields of arbitrary 3d nanostructures. *Nano letters*, 20(1):329–338, 2019.
- [26] Tianju Xue, Alex Beatson, Sigrid Adriaenssens, and Ryan Adams. Amortized finite element analysis for fast pde-constrained optimization. In *International Conference on Machine Learning*, pages 10638–10647. PMLR, 2020.
- [27] Yuehaw Khoo and Lexing Ying. Switchnet: a neural network model for forward and inverse scattering problems. *SIAM Journal on Scientific Computing*, 41(5):A3182–A3201, 2019.

- [28] Luca Grementieri and Paolo Galeone. Towards neural sparse linear solvers. *arXiv preprint arXiv:2203.06944*, 2022.
- [29] Jun-Ting Hsieh, Shengjia Zhao, Stephan Eismann, Lucia Mirabella, and Stefano Ermon. Learning neural PDE solvers with convergence guarantees. In *International Conference on Learning Representations*, 2018.
- [30] Tobias Pfaff, Meire Fortunato, Alvaro Sanchez-Gonzalez, and Peter Battaglia. Learning mesh-based simulation with graph networks. In *International Conference on Learning Representations*, 2020.
- [31] Gabrio Rizzuti, Ali Siahkoobi, and Felix J Herrmann. Learned iterative solvers for the Helmholtz equation. In *81st EAGE Conference and Exhibition 2019*, volume 2019, pages 1–5. European Association of Geoscientists & Engineers, 2019.
- [32] Yuyan Chen, Bin Dong, and Jinchao Xu. Meta-MgNet: Meta multigrid networks for solving parameterized partial differential equations. *Journal of Computational Physics*, 455:110996, 2022.
- [33] Yael Azulay and Eran Treister. Multigrid-augmented deep learning preconditioners for the helmholtz equation. *SIAM Journal on Scientific Computing*, (0):S127–S151, 2022.
- [34] Bar Lerer, Ido Ben-Yair, and Eran Treister. Multigrid-augmented deep learning for the Helmholtz equation: Better scalability with compact implicit layers. *arXiv preprint arXiv:2306.17486*, 2023.
- [35] Yann LeCun, Léon Bottou, Yoshua Bengio, and Patrick Haffner. Gradient-based learning applied to document recognition. *Proceedings of the IEEE*, 86(11):2278–2324, 1998.
- [36] Olaf Ronneberger, Philipp Fischer, and Thomas Brox. U-net: Convolutional networks for biomedical image segmentation. In *Medical Image Computing and Computer-Assisted Intervention–MICCAI 2015: 18th International Conference, Munich, Germany, October 5–9, 2015, Proceedings, Part III 18*, pages 234–241. Springer, 2015.
- [37] Juncai He and Jinchao Xu. MgNet: A unified framework of multigrid and convolutional neural network. *Science china mathematics*, 62:1331–1354, 2019.
- [38] Remi Lam, Alvaro Sanchez-Gonzalez, Matthew Willson, Peter Wirnsberger, Meire Fortunato, Ferran Alet, Suman Ravuri, Timo Ewalds, Zach Eaton-Rosen, Weihua Hu, et al. Learning skillful medium-range global weather forecasting. *Science*, page eadi2336, 2023.
- [39] Gene H Golub and Charles F Van Loan. *Matrix computations*. JHU press, 2013.
- [40] Ulrich Trottenberg, Cornelius W Oosterlee, and Anton Schuller. *Multigrid*. Elsevier, 2000.
- [41] Vincent Dumoulin and Francesco Visin. A guide to convolution arithmetic for deep learning. *arXiv preprint arXiv:1603.07285*, 2016.
- [42] Stig Larsson and Vidar Thomée. *Partial differential equations with numerical methods*, volume 45. Springer, 2003.
- [43] Sin-I Cheng and Gregory Shubin. Computational accuracy and mesh reynolds number. *Journal of Computational Physics*, 28(3):315–326, 1978.
- [44] Jun Zhang. Accelerated multigrid high accuracy solution of the convection-diffusion equation with high reynolds number. *Numerical Methods for Partial Differential Equations: An International Journal*, 13(1):77–92, 1997.
- [45] Murli M Gupta, Jules Kouatchou, and Jun Zhang. A compact multigrid solver for convection-diffusion equations. *Journal of Computational Physics*, 132(1):123–129, 1997.
- [46] LONG Chen. Finite difference method for stokes equations: Mac scheme. *University of California, Irvine <https://www.math.uci.edu/~chenlong/226/MACStokes.pdf>*, 2016.

- [47] Adam Paszke, Sam Gross, Francisco Massa, Adam Lerer, James Bradbury, Gregory Chanan, Trevor Killeen, Zeming Lin, Natalia Gimelshein, Luca Antiga, et al. Pytorch: An imperative style, high-performance deep learning library. *Advances in neural information processing systems*, 32, 2019.
- [48] Alex Krizhevsky, Geoffrey Hinton, et al. Learning multiple layers of features from tiny images. 2009.
- [49] Han Xiao, Kashif Rasul, and Roland Vollgraf. Fashion-mnist: a novel image dataset for benchmarking machine learning algorithms. *arXiv preprint arXiv:1708.07747*, 2017.
- [50] Yann LeCun. The mnist database of handwritten digits. <http://yann.lecun.com/exdb/mnist/>, 1998.